World Scientific
www.worldscientific.com

Mapping the small-world properties of brain networks in Chinese to English simultaneous interpreting by using functional near-infrared spectroscopy

Xiaohong Lin*, Victoria Lai Cheng Lei[†,‡], Defeng Li[†,‡], Zhishan Hu*,
Yutao Xiang* and Zhen Yuan[*,§]

*Faculty of Health Sciences
University of Macau, Macau SAR, P. R. China

†Department of English
Faculty of Arts and Humanities
University of Macau, Macau SAR, P. R. China

‡Centre for Studies of Translation
Interpreting and Cognition
University of Macau, Macau
§zhenyuan@umac.mo

The aim of this study is to examine the small-world properties of functional brain networks in Chinese to English simultaneous interpreting (SI) using functional near-infrared spectroscopy (fNIRS). In particular, the fNIRS neuroimaging combined with complex network analysis was performed to extract the features of functional brain networks underling three translation strategies associated with Chinese to English SI: "transcoding" that takes the "shortcut" linking translation equivalents between Chinese and the English, "code-mixing" that basically does not involve bilingual processing, and "transphrasing" that takes the "long route" involving a monolingual processing of meaning in Chinese and then another monolingual processing of meaning in English. Our results demonstrated that the small-world network topology was able to distinguish well between the transcoding, code-mixing and transphrasing strategies related to Chinese to English SI.

Keywords: fNIRS; translation; simultaneous interpreting; small-world; brain network.

§Corresponding author.

1. Introduction

Simultaneous interpreting (SI) is widely adopted for international communication, which involves a series of cognitive tasks related to language processing across two languages.[1,2] Previous studies demonstrated that there were three alternative strategies for bilinguals to translate between languages, i.e., "transcoding" which is memory-based and takes the "shortcut" linking translation equivalents between the source language (SL) and the target language (TL), "transphrasing" which is meaning-based and takes the "long route", and "code-mixing" which retains the SL form in the TL production and thus probably involves hardly any bilingual processing effort. More importantly, the functional neuroimaging technologies make themselves ideal candidates for measuring the cognitive effort involved in various translation strategies. To date, only two neuroimaging studies have been performed to examine the brain activation associated with SI using professional interpreters,[2,3] which discovered that the brain activation in the left hemisphere including the Broca's area exhibited significant relationship with SI.[3–6] However, the previous works mainly focused on identifying the brain activation patterns associated with SI between two phonographic languages rather than two incongruent languages (i.e., English versus Chinese). Meanwhile, advances in the investigation of neural mechanism are experiencing a transition from identifying the brain activation regions to constructing functional brain networks. In particular, complex network analysis has been proposed to examine the small-world and scale-free characteristics of brain networks underlying cognition functions or various neurological and psychiatric disorders.[7–11]

The aim of this present study is to inspect the small-world properties of functional brain networks in SI between two incongruent languages (English versus Chinese). In addition, we will study the topological and spatial features of local brain networks according to three different translation strategies associated with Chinese to English SI, which include transcoding, code-mixing, and transphrasing. More importantly, we will construct and analyze the functional brain networks of the three translation strategies related to Chinese to English SI using functional near-infrared spectroscopy (fNIRS) measurements.[12–14] Small-world network characteristics including the clustering coefficient, average path length, and average node degree of brain network will be explored and compared between the various translation strategies. Since the small-world properties of brain networks regarding the three translation strategies have not been explored, this pilot work will definitely pave a new avenue for better understanding of the neural mechanism of Chinese to English SI.

2. Materials and Methods

2.1. *Participants*

Ten postgraduate students (bilingual) from the University of Macau (UM) whose major was Translation Studies took part in this study (six females, mean age = 24 years, SD = 2.21 years). All bilingual participants had a very high proficiency in both written and spoken English (TEM-8) and had received training in Chinese to English SI over half a year. All participants were right-handed with normal or corrected-to-normal vision. Participants with reported histories of neurological or psychiatric disorders were excluded from this study. All participants were required to sign informed consent documents prior to the experimental tests. The protocol for the clinical trial was approved by the Ethics Committees of UM and were carried out in accordance with the approved guidelines.

2.2. *Stimuli and procedures*

The stimulus materials were all two-character cultural-specific items selected from the UM Magazine (Chinese version). The corpus contains totally 159,058 characters, 3983 common nouns, and 1869 culture-specific items. In this study, we used two-character words as stimuli materials to ensure that the participants only used one SI strategy to translate each stimulus material. From the culture-specific items in the corpus, 15 were selected for task one (transcoding), 15 for task two (code-mixing), and 15 for task three (transphrasing). Each task included 15 trials and each trial lasted 22 s, which included a pre-stimulus period of 1 s with a red fixation cross presented in the center of the screen of the monitor, a stimulus period of 1 s, and then a post-stimulus and recovery period of 20 s with a white fixation cross displayed in the center of the
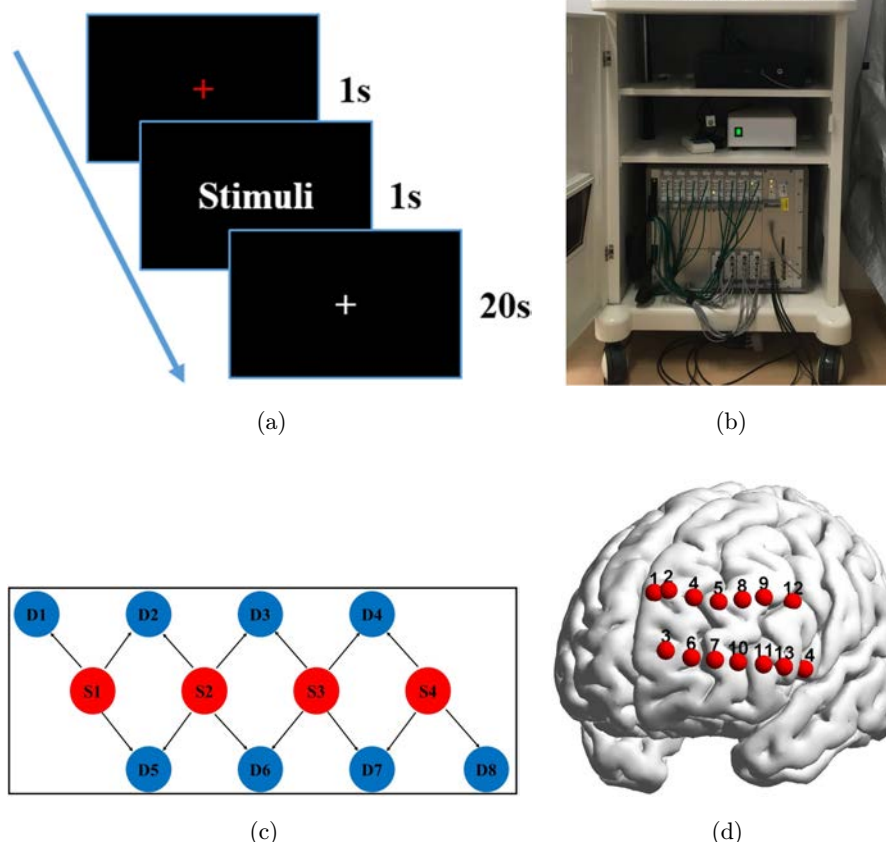
Fig. 1. (a) Schematic of the experimental design. (b) The CW6 fNIRS system. (c) The configurations of the source and detector pairs. (d) Locations of the 14 fNIRS channels along the frontal cortex.

screen of the monitor [Fig. 1(a)]. It took about 20 min to finish the data acquisition.

For task one, participants were required to translate orally the two-character culture-specific Chinese items displayed on the computer screen into English. Since the competent bilingual participants had received training in SI, they should go for the "shortcut" (transcoding) and gain access to the translation equivalent in English. For task two, participants needed to translate the items orally into English using the nontranslation (code-mixing), i.e., producing the sound of the Chinese item rather than giving its direct equivalent in English. For task three, participants were instructed to do the translation based on transphrasing, i.e., explaining what/where

the item is rather than giving its direct equivalent in English.

2.3. fNIRS data recording and pre-processing

The experimental tests were performed with a continuous wave (CW) fNIRS system (CW6 fNIRS system; TechEn Inc., Milford, MA) [Fig. 1(b)]. This system that has four laser sources at wavelengths 690 nm and 830 nm and eight optical detectors can measure the changes in both HbO and HbR concentrations in the human brain. The fNIRS optodes were placed on a home-made plastic patch (6 cm × 18 cm) covering the left frontal cortex (region of

Table 1. The mean MNI coordinates for all the 14 channels across all subjects.

Channels	x	y	z
Ch1	-5 ± 6	65 ± 4	30 ± 8
Ch2	-14 ± 3	64 ± 4	30 ± 7
Ch3	-18 ± 3	72 ± 2	8 ± 8
Ch4	-24 ± 3	60 ± 5	30 ± 6
Ch5	-34 ± 3	54 ± 6	30 ± 7
Ch6	-29 ± 4	67 ± 3	7 ± 7
Ch7	-39 ± 4	60 ± 5	6 ± 7
Ch8	-43 ± 3	44 ± 7	29 ± 6
Ch9	-50 ± 3	34 ± 8	29 ± 5
Ch10	-48 ± 3	50 ± 7	4 ± 6
Ch11	-54 ± 3	39 ± 7	2 ± 5
Ch12	-57 ± 3	21 ± 9	27 ± 5
Ch13	-57 ± 3	25 ± 10	1 ± 5
Ch14	-61 ± 4	7 ± 11	-2 ± 6

interest), which was able to generate 14 channels, as shown in Fig. 1(c). Additionally, a three-dimensional (3D) magnetic space digitizer Patriot Digitizer (Polhemus Inc.) was used to measure the 3D spatial coordinates of each optode, and then a probabilistic registration method based on NIRS-SPM software was adopted to access each channel's corresponding coordinates in the Montreal Neurological Institute (MNI) space[15] as displayed in Fig. 1(d). The mean MNI coordinates across all subjects were provided in Table 1. The distance between each source and each detector was 3 cm and the fNIRS sampling rate was kept at 50 Hz.

The fNIRS data preprocessing was implemented using Homer2_UI software (v1.5.2).[16] The raw fNIRS data were first converted to optical density changes, and then to HbO and HbR concentration changes at different time points using Modified Beer–Lambert law.[17] A low pass filter of 0.2 Hz was performed for the generated data followed by a high pass filter of 0.015 Hz. In this study, only HbO data were analyzed due to its high signal-to-noise ratio.[18] The trial-averaged HbO signals from each channel were used to construct the brain network for each participant. The grand-averaged HbO data for each channel were calculated and plotted in Fig. 2.

2.4. Network construction and analysis

In this study, the fNIRS channel is denoted as the node of the brain network while the edge is defined as the Pearson correlation coefficient generated from the measurements between any two channels. Importantly, the correlation coefficient of two run-averaged time series (the HbO signals of any two fNIRS channels) is considered as the functional connectivity between the two nodes of the brain networks.[19,20] To analyze the properties of the network topology constructed by all nodes based on graph theory, we computed the correlation coefficients among all 14 channels and then generated the correlation coefficient matrix. During the process of constructing brain networks, we need to binarize the correlation coefficient matrix by setting a threshold T. As a result, the element value of the matrix is set to 0 when the absolute value of Pearson correlation coefficient is smaller than T, which should not be considered as significant connectivity. If this is the case, the edges can be considered as nonexistent in the network analysis. By contrast,
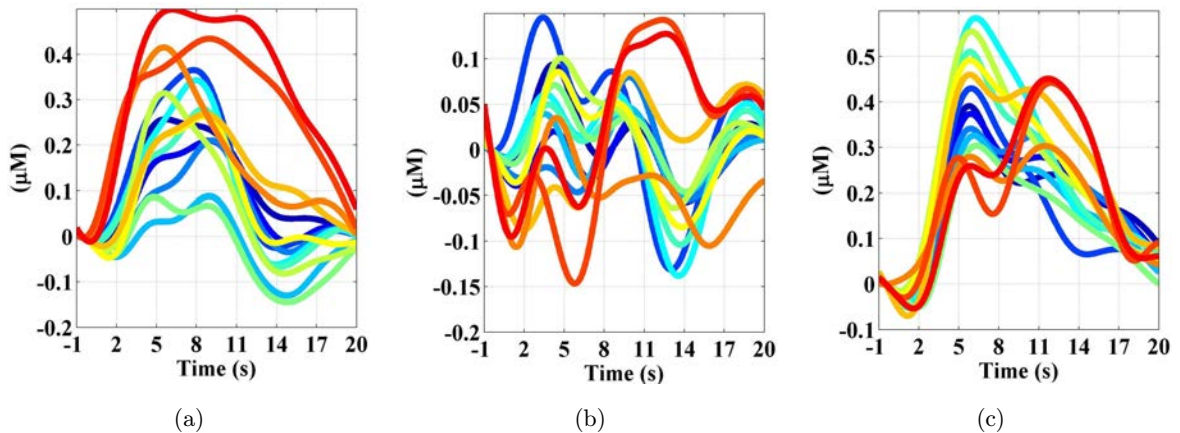

Fig. 2. Grand-averaged HbO data across all subjects associated with: (a) the transcoding strategy, (b) the code-mixing strategy, and (c) the transphrasing strategy for all 14 channels.

the element value should be set to 1 when the absolute value of the correlation coefficient is larger than or equal to T.[21] To further facilitate converting the binary matrix into visualization networks, the values of binary matrix as edges of brain networks are mapped to the 3D space by using the BrainNet Viewer tool.[22]

2.5. *Characteristic indices of the networks*

The indicators of complex networks including the clustering coefficient, average path length, average node degree, and measure of small-world network are usually used to access the network topology characteristics. Interestingly, these indicators can be generated from the acquired binary matrix of nodes. For example, the clustering coefficient of the network is denoted as[23,24]

$$C_{\text{net}} = \sum_{i \in G} \frac{E_i}{K_i(K_{i-1})} \bigg/ N, \qquad (1)$$

in which N is the number of nodes, G is the set of all nodes in the network, E_i is the number of edges in the subgraph G_i, and G_i is defined as the graph including the nodes that are the direct neighbors of the ith node, i.e., directly connected to the ith node with an edge.[10] K_i is the number of nodes directly connected to the node i, which is defined as the degree of node i.

In particular, the average node degree of network K_{net} is defined as the mean of degrees from all nodes within the network.[24]

Meanwhile, the average path length of network is specified as[23,24]

$$L_{\text{net}} = \sum_{i \in G} \frac{\sum_{i \neq j \in G} \min\{L_{i,j}\}}{N - 1} \bigg/ N, \qquad (2)$$

in which $\min\{L_{i,j}\}$ is the shortest path (geodesic) between node i and node j.

The measure of small-worldness is denoted as[24,25]

$$\sigma = \frac{C_{\text{net}}/C_{\text{random}}}{L_{\text{net}}/L_{\text{random}}}, \qquad (3)$$

in which C_{random} and L_{random} are the clustering coefficient and average path of random networks that correspond to the clustering coefficient C_{net} and average path length L_{net} of the brain networks, respectively. In addition, the Markov chain algorithm is used to generate 100 random networks with the degree sequences that correlate with the binary matrix. And then, the mean clustering coefficient and averaged path length from the 100 random networks are denoted as the clustering coefficient and average path of random network, respectively.[10,21,26–28]

3. Results

3.1. *Pearson correlation coefficient matrix, binary matrix, and 3D brain networks*

In this study, we examined the attributes of generated brain networks associated with three Chinese to English SI strategies including transcoding, code-mixing, and transphrasing by using fNIRS recordings.

Figures 3(a1)–3(a5), 3(b1)–3(b5), and 3(c1)–3(c5) display the calculated Pearson correlation coefficient matrix, binary matrix, and 3D brain networks for the transcoding, code-mixing, and transphrasing strategy, respectively. In particular, Figs. 3(a1), 3(b1) and 3(c1) present the mean correlation coefficients across all participants for the three cases, in which the horizontal and vertical axes denote the nodes while the elements within the square areas represent the correlation coefficient between the two nodes. In addition, the binary matrix in Figs. 3(a2) and 3(a4), 3(b2) and 3(b4), and 3(c2) and 3(c4), are, respectively, constructed by using the results in Figs. 3(a1), 3(b1) and 3(c1) with threshold values of 0.2 and 0.5 for the three cases, in which the white regions exhibited the significant connection. Further, Figs. 3(a3) and 3(a5), 3(b3) and 3(b5), and 3(c3) and 3(c5) show the visualization of the networks in 3D for the binary matrix in Figs. 3(a2) and 3(a4), 3(b2) and 3(b4), and 3(c2) and 3(c4), respectively.

3.2. *Network metrics generated with absolute thresholding*

Meanwhile, the network properties were generated and compared between the three SI strategies with various thresholds (absolute thresholding), which were ranged from 0.2 to 0.74.[10,29] More importantly, the paired two-sample t-tests were also performed between any two of the three cases and the analysis results were provided in Figs. 4–6.
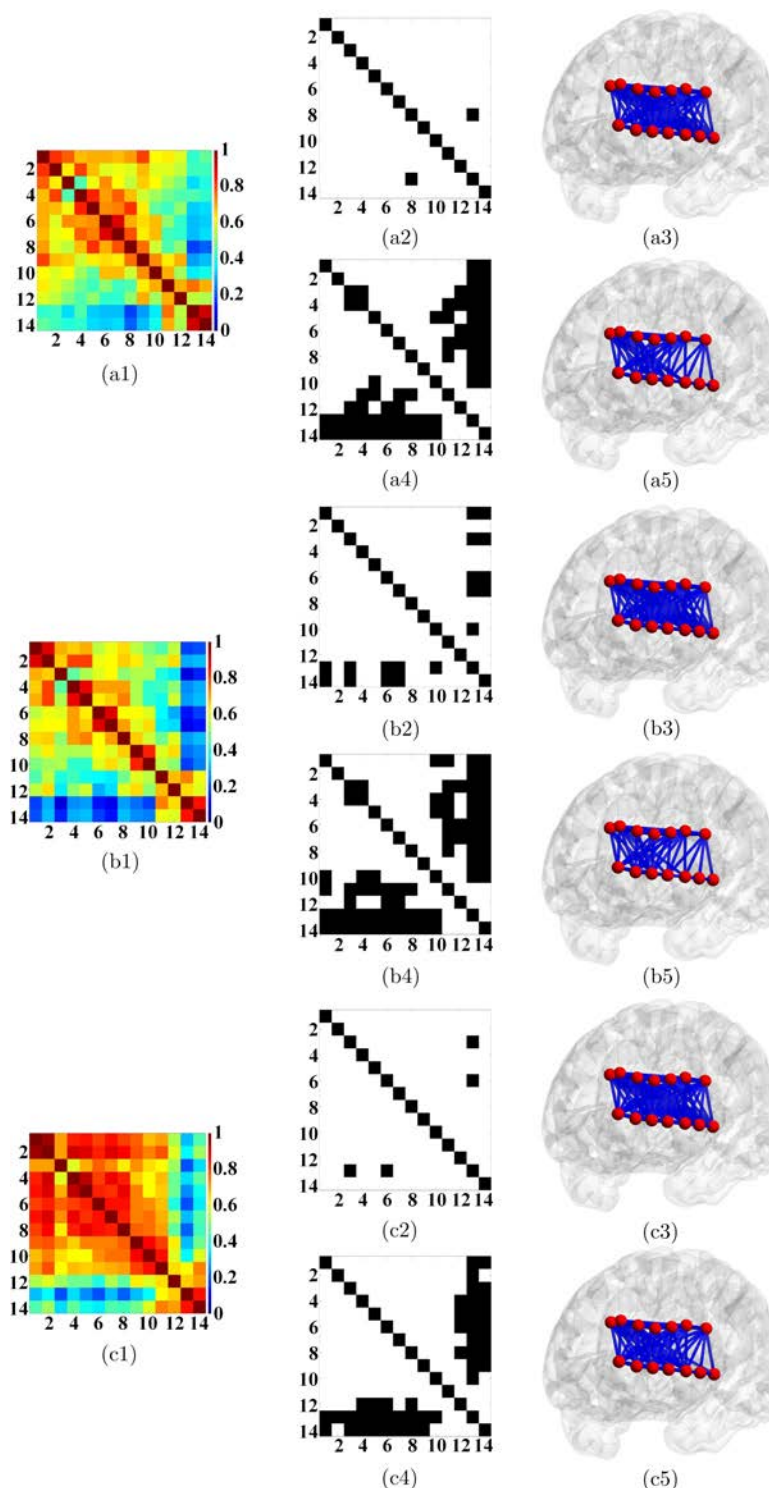
Fig. 3. Correlation coefficients, binary matrix and 3D relative networks of brain nodes for the transcoding, code-mixing and transphrasing translation strategies. (a1)–(a5) are for the transcoding case: (a1) are the correlation coefficients, (a2) and (a3) are the binary matrix and brain network with the threshold value of 0.2, and (a4) and (a5) are the binary matrix and brain network with the threshold value of 0.5. (b1)–(b5) are for the code-mixing case: (b1) are the correlation coefficients, (b2) and (b3) are the binary matrix and brain network with the threshold value of 0.2, and (b4) and (b5) are the binary matrix and brain network with the threshold value of 0.5. (c1)–(c5) are for the transphrasing case: (c1) are the correlation coefficients, (c2) and (c3) are the binary matrix and brain network with the threshold value of 0.2, and (c4) and (c5) are the binary matrix and brain network with the threshold value of 0.5.
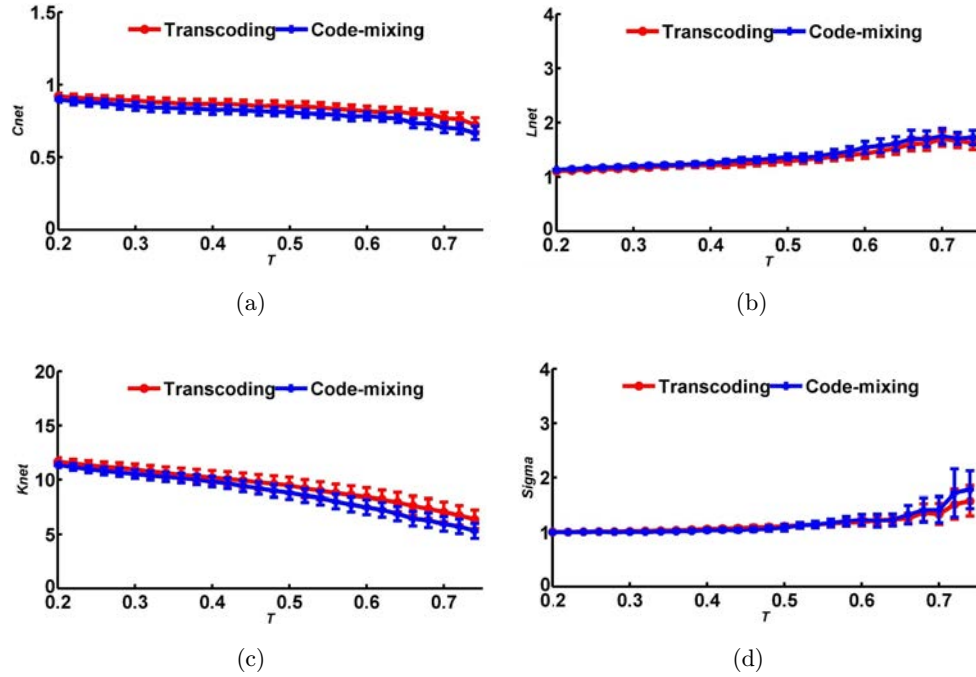
Fig. 4. Comparison of the small-world indicators between the transcoding and code-mixing translation strategies with absolute thresholding: (a) the clustering coefficient, (b) average path length, (c) average node degree and (d) measure of small-worldness. The curves (mean $\pm$ SE) show the network indicators with different thresholds, in which the red and blue color represent the transcoding and code-mixing strategy respectively. The horizontal axes denote the threshold values whereas the vertical axes denote the network property indexes.
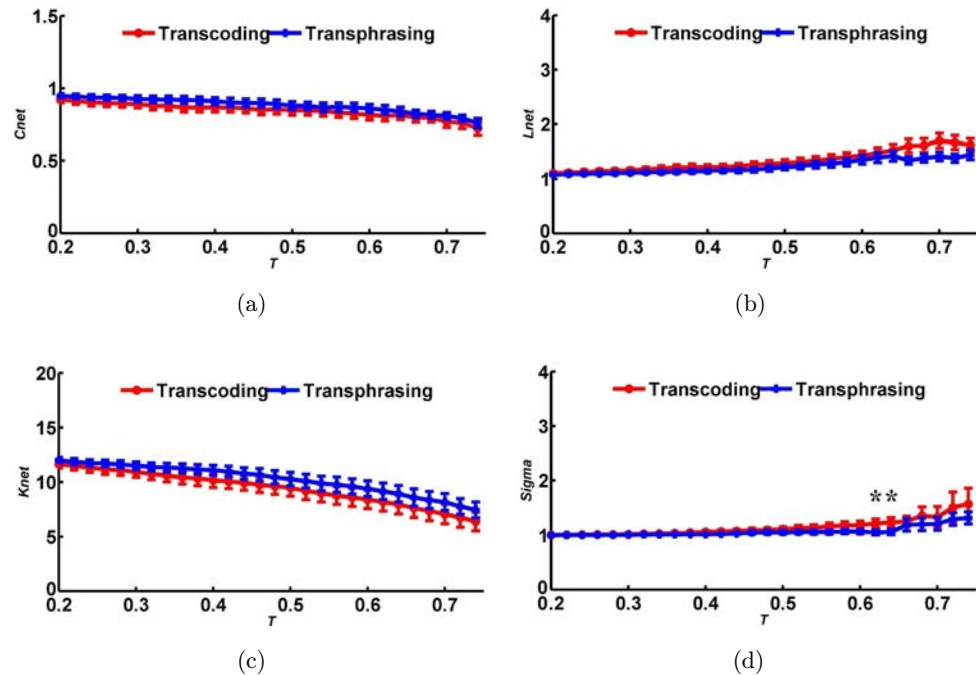*$p < 0.05$.

Fig. 5. Comparison of the small-world indicators between the transphrasing and transcoding translation strategy with absolute thresholding: (a) the clustering coefficient, (b) average path length, (c) average node degree and (d) measure of small-worldness. The curves (mean $\pm$ SE) show the network indicators with different thresholds, in which the red and blue color represent the transcoding and transphrasing strategy respectively. The horizontal axes denote the threshold values whereas the vertical axes denote the network property indexes.
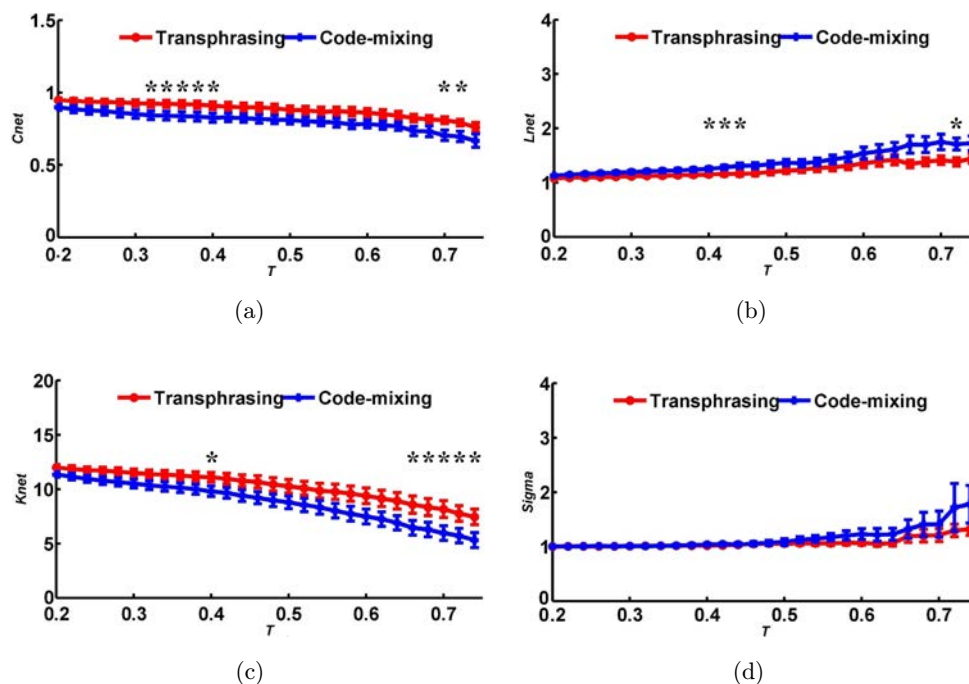*$p < 0.05$.

Fig. 6. Comparison of the small-world indicators between the transphrasing and code-mixing translation strategy with absolute thresholding: (a) the clustering coefficient, (b) average path length, (c) average node degree and (d) measure of small-worldness. The curves (mean $\pm$ SE) show the network indicators with different thresholds, in which the red and blue color represent the transphrasing and code-mixing strategy respectively. The horizontal axes denote the threshold values whereas the vertical axes denote the network property indexes.
*$p < 0.05$.

Interestingly, according to Figs. 4(a) and 4(c) the transcoding case exhibited larger network clustering coefficients and higher average node degrees as compared to those of code-mixing case across all thresholds used. However, the average path lengths of the networks from code-mixing case were larger than that of transcoding case for all threshold values used, as plotted in Fig. 4(b). The higher clustering coefficient and higher average node degree of the network indicated that the brain nodes of transcoding case had much closer and denser connections than those from the code-mixing, whereas the lower average path length demonstrated that transcoding case had more efficient connections. Interestingly, if the network has the small-world properties, the measure of small-worldness should be larger than 1.[30,31] The results in Fig. 4(d) exhibited that local brain networks for both the transcoding and code-mixing cases had small-world characteristics. Interestingly, the measure of small-worldness increased with the increased threshold values. In particular, we discovered that the measure of small-worldness (the small-world property index) for code-mixing case was larger

than that of transcoding case when the threshold was higher than 0.5.

In addition, as shown in Fig. 5, the transcoding and transphrasing cases also exhibited significant differences in the clustering coefficient, average path length, average node degree, and measure of small-worldness. According to the three network metrics including the clustering coefficient, average path length, and average node degree of the network, the transphrasing case showed higher efficiency and denser connections as compared to those from the transcoding case. Interestingly, the small-world property index of transcoding case was larger than that from the transphrasing one although both exhibited the small-world characteristics.

Furthermore, we discovered from Fig. 6 that in terms of the three network metrics including the clustering coefficient, average path length, and average node degree of the network, the transphrasing SI strategy showed higher efficiency and stronger density in brain connectivity between nodes of networks than the code-mixing strategy. By contrast, the small-world property index of

code-mixing case was larger than that of trans-phrasing case.

3.3. Network metrics generated with relative thresholding

In addition, the network metrics were also generated for the three SI strategies with various network densities (relative thresholding). For the present work, the thresholds of sparsity (network density) ranged between 40% and 57% with an interval of 1% because networks with wide sparsity band can exhibit the small-world properties.[32–34] Likewise, the paired two-sample *t*-tests were also conducted between the three cases and the analysis results are displayed in Figs. 7–9.

We discovered from Fig. 7(a) that the transcoding case exhibited larger network clustering coefficients as compared to those of code-mixing case for all sparsity values used although they showed no difference in the average path lengths of the networks as plotted in Fig. 7(b). In particular, as plotted in Fig. 7(c), the measure of small-worldness of transcoding case was larger than that of code-mixing case for all thresholds.

Interestingly, it was discovered from Fig. 8 that the transcoding case showed larger network clustering coefficient and small-world property index than those of transphrasing case.

However, as shown in Fig. 9, the transphrasing case exhibited larger network clustering coefficients and stronger small-world property index as compared
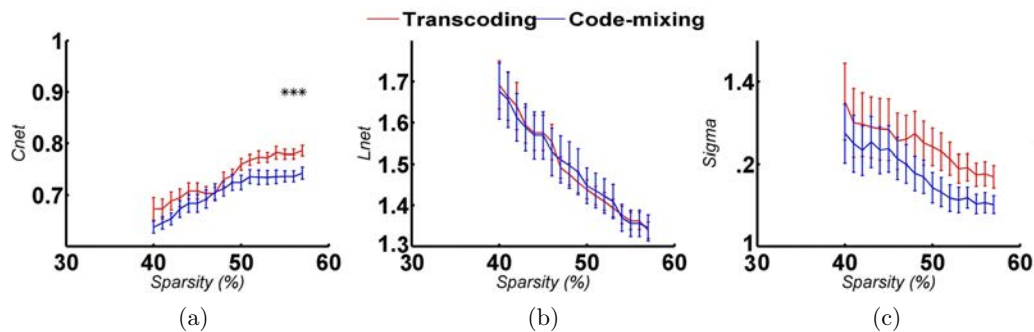

Fig. 7. Comparison of the small-world indicators between the transcoding and code-mixing translation strategies with relative thresholding: (a) the clustering coefficient, (b) average path length and (c) measure of small-worldness. The curves (mean $\pm$ SE) show the network indicators with different sparsity, in which the red and blue color represent the transcoding and code-mixing strategy respectively. The horizontal axes denote the sparsity values whereas the vertical axes denote the network property indexes. *$p < 0.05$.
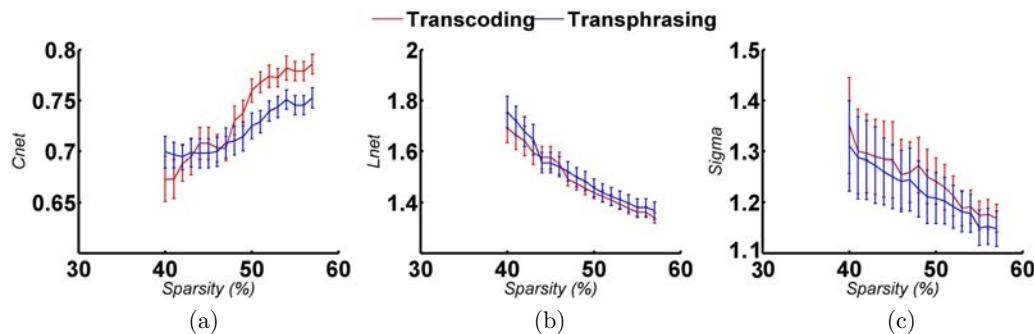

Fig. 8. Comparison of the small-world indicators between the transcoding and transphrasing translation strategy with relative thresholding: (a) the clustering coefficient, (b) average path length and (c) measure of small-worldness. The curves (mean $\pm$ SE) show the network indicators with different thresholds, in which the red and blue color represent the transcoding and transphrasing strategy respectively. The horizontal axes denote the sparsity values whereas the vertical axes denote the network property indexes.
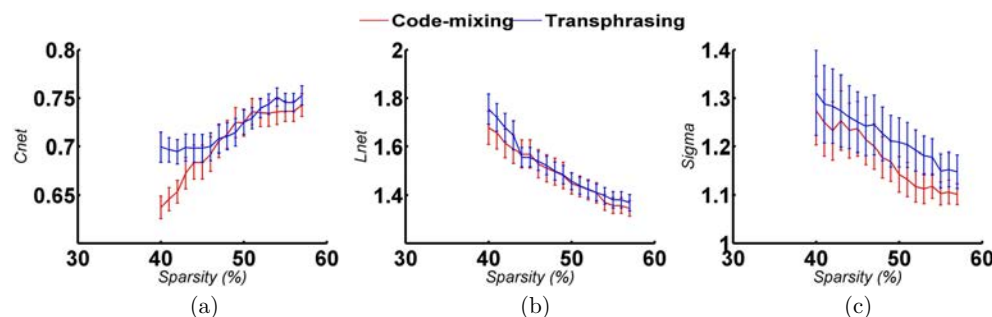
Fig. 9. Comparison of the small-world indicators between the code-mixing and transphrasing translation strategy with relative thresholding: (a) the clustering coefficient, (b) average path length and (c) measure of small-worldness. The curves (mean ± SE) show the network indicators with different sparsity, in which the red and blue color represent the code-mixing and transphrasing strategy respectively. The horizontal axes denote the sparsity values whereas the vertical axes denote the network property indexes.

to those of code-mixing case for most of the sparsity values used although this is not the case for the average path lengths.

4. Discussion

It is widely recognized that for complex network analysis, the clustering coefficient of network denotes the local efficiency or small group in information transfer of network.[35] By contrast, the average path length of network describes the global efficiency and the ability of parallel information transmission of network, in which a large average path length correlates with a low efficiency.[35] In addition, the average node degree represents the network density, in which the network connections are sparse when the average node degree is small while the network connections are dense when the average node degree is large.[30] Further, the small-world property index is to examine whether the brain networks exhibit the small-world properties.[10,35]

4.1. Network properties with absolute thresholding

We discovered from Figs. 4–6 that the brain networks of transphrasing case showed the larger clustering coefficient, the shorter average path length, and the greater average node degree than those of code-mixing case. Meanwhile, the transphrasing case exhibited higher efficiency and denser connections as compared to the transcoding case. Likewise, the transcoding case also exhibited larger network clustering coefficient and higher average node degrees as compared to those of code-mixing

case. However, the small-world property index of transphrasing case exhibited stronger randomness than that of transcoding or code-mixing case. These results demonstrate that there exists significant difference between the neural mechanisms of the three SI strategies from the perspective of the network. We discovered that in terms of the measures of three network metrics including the clustering coefficient, average path length, and average node degree of the network, the transphrasing case showed the highest efficiency and densest connections as compared to those from the transcoding and code-mixing cases, whereas the code-mixing case showed the lowest efficiency. These neural findings were in line with previous results that transphrasing case involved more complex cognitive effort than the transcoding case.[36,37] However, this is not the case for the code-mixing strategy, which does not involve significant cognitive effort at all. Interestingly, our findings also demonstrated and validated that the professional interpreters are more likely to adopt the transcoding and code-mixing strategies than the transphrasing one in order to improve the SI efficiency.

4.2. Network properties with relative thresholding

According to the analysis results in Figs. 7–9 based on the relative thresholding, we discovered that both the transcoding and transphrasing cases showed larger clustering coefficient than that of code-mixing case although only the transcoding case exhibited the significance. These observations showed good agreement with those from the absolute thresholding. By contrast, the code-mixing case

exhibited stronger randomness than those of transcoding and transphrasing cases, which were totally different from the results generated from the absolute thresholding. Interestingly, the average path length showed no difference between the three SI cases although that from the absolute thresholding exhibited significant difference.

In addition, it should be pointed out that the distance between each source and each detector was set as 3 cm, which can eliminate or reduce the effect of optical path length in CW6 fNIRS system across various subjects and channels. The optical path length was generally considered as a constant for most of the analysis cases since fNIRS technique, as a signal processing method, was not involved in accurate source localization in 3D space.

In summary, fNIRS is a facilitating tool for exploring and building functional brain network associated with Chinese to English SI. In this study, we combined fNIRS neuroimaging technique with the complex network theory to analyze and compare the attribute features of functional brain networks in the left frontal region for three translation strategies including transcoding, code-mixing, and transphrasing. We discovered that the functional brain activation networks for transphrasing strategy exhibited the largest clustering coefficient, the shortest average path length, and the greatest average node degree as compared to those from the code-mixing or transcoding strategy.

Conflict of Interest

The authors have non-financial associations that may be relevant or seen as relevant to the submitted manuscript.

Acknowledgments

References

1. A. G. Hervais-Adelman, B. Moser-Mercer, N. Golestani, "Executive control of language in the bilingual brain: Integrating the evidence from neuroimaging to neuropsychology," *Front. Psychol.* **2**, 234 (2011).

2. M. Becker, T. Schubert, T. Strobach, J. Gallinat, S. Kühn, "Simultaneous interpreters vs. professional multilingual controls: Group differences in cognitive control as well as brain structure and function," *NeuroImage* **134**, 250–260 (2016).

3. J. O. Rinne, J. Tommola, M. Laine, B. J. Krause, D. Schmidt, V. Kaasinen, M. Teräs, H. Sipilä, M. Sunnari, "The translating brain: Cerebral activation patterns during simultaneous interpreting," *Neurosci. Lett.* **294**(2), 85–88 (2000).

4. D. Klein, B. Milner, R. J. Zatorre, E. Meyer, A. C. Evans, "The neural substrates underlying word generation: A bilingual functional-imaging study," *Proc. Natl. Acad. Sci. USA* **92**(7), 2899–2903 (1995).

5. V. Quaresima, M. Ferrari, M. C. van der Sluijs, J. Menssen, W. N. Colier, "Lateral frontal cortex oxygenation changes during translation and language switching revealed by non-invasive near-infrared multi-point measurements," *Brain Res. Bull.* **59**(3), 235–243 (2002).

6. L. A. Petitto, M. Berens, I. Kovelman, M. H. Dubins, K. Jasinska, M. Shalinsky, "The "Perceptual Wedge Hypothesis" as the basis for bilingual babies' phonetic processing advantage: New insights from fNIRS brain imaging," *Brain Lang.* **121**(2), 130–143 (2012).

7. M. Rubinov, S. A. Knock, C. J. Stam, S. Micheloyannis, A. W. Harris, L. M. Williams, M. Leanne, M. Breakspear, "Small-world properties of nonlinear brain activity in schizophrenia," *Hum. Brain Mapp.* **30**(2), 403–416 (2009).

8. T. Uehara, T. Yamasaki, T. Okamoto, T. Koike, S. Kan, S. Miyauchi, J. Kira, S. Tobimatsu, "Efficiency of a "small-world" brain network depends on consciousness level: A resting-state fMRI study," *Cereb. Cortex* **24**(6), 1529–1539 (2013).

9. S. Achard, E. Bullmore, "Efficiency and cost of economical brain functional networks," *PLoS Comput. Biol.* **3**(2), 17 (2017).

10. J. R. Ding, W. Liao, Z. Zhang, D. Mantini, Q. Xu, G. R. Wu, G. Lu, H. Chen, "Topological fractionation of resting-state networks," *Plos One* **6**(10), e26596 (2011).

11. L. Pessoa, "Understanding brain networks and brain organization," *Phys. Life Rev.* **11**(3), 400–435 (2014).

12. X. Liu, K. Hong, "Detection of primary RGB colors projected on a screen using fNIRS," *J. Innov. Opt. Health Sci.* **10**(3), 1750006 (2017).

13. T. Li, Y. Li, Y. Sun, M. Duan, L. Peng, "Effect of head model on Monte Carlo modeling of spatial sensitivity distribution for functional near-infrared spectroscopy," *J. Innov. Opt. Health Sci.* **8**(5), 1550024 (2015).

14. Z. Deng, Q. Huang, J. Huang, W. Zhang, C. Qi, X. Xu, "Association between central obesity and

executive function as assessed by stroop task performance: A functional near-infrared spectroscopy study," *J. Innov. Opt. Health Sci.* **11**(1), 1750010 (2018).

15. A. K. Singh, M. Okamoto, H. Dan, V. Jurcak, I. Dan, "Spatial registration of multichannel multisubject fNIRS data to MNI space without MRI," *NeuroImage* **27**(4), 842–851 (2005).

16. T. J. Huppert, S. G. Diamond, M. A. Franceschini, D. A. Boas, "HomER: A review of time-series analysis methods for near-infrared spectroscopy of the brain," *Appl. Opt.* **48**(10), 280–298 (2009).

17. M. Cope, D. T. Delpy, "System for long-term measurement of cerebral blood and tissue oxygenation on newborn infants by near infra-red transillumination," *Med. Biol. Eng. Comput.* **26**(3), 289–294 (1988).

18. J. Zhang, X. Lin, G. Fu, L. Sai, H. Chen, J. Yang, M. Wang, Q. Liu, G. Yang, J. Zhang, "Mapping the small-world properties of brain networks in deception with functional near-infrared spectroscopy," *Sci. Rep.* **6**, 25297 (2016).

19. K. J. Friston, "Functional and effective connectivity in neuroimaging: A synthesis," *Hum. Brain Mapp.* **2**, 56–78 (1994).

20. B. Biswal, Y. F. Zerrin, V. M. Haughton, J. S. Hyde, "Functional connectivity in the motor cortex of resting human brain using echo-planar mri," *Magn. Reson. Med.* **34**(4), 537–541 (1995).

21. W. Liao, Z. Zhang, Z. Pan, D. Mantini, J. Ding, X. Duan, C. Luo, G. Lu, H. Chen, "Altered functional connectivity and small-world in mesial temporal lobe epilepsy," *PloS One* **5**(1), 8525 (2010).

22. M. Xia, J. Wang, Y. He, "BrainNet Viewer: A network visualization tool for human brain connectomics," *PloS One* **8**(7), 68910 (2013).

23. D. J. Watts, S. H. Strogatz, "Collective dynamics of 'small-world' networks," *Nature* **393**(6684), 440 (1998).

24. M. Rubinov, O. Sporns, "Complex network measures of brain connectivity: Uses and interpretations," *NeuroImage* **52**(3), 1059–1069 (2010).

25. M. D. Humphries, K. Gurney, "Network 'small-world-ness': A quantitative method for determining canonical network equivalence," *PloS One* **3**(4), 0002051 (2008).

26. S. Maslov, K. Sneppen, "Specificity and stability in topology of protein networks," *Science* **296**(5569), 910–913 (2002).

27. S. Hayasaka, P. J. Laurienti, "Comparison of characteristics between region- and voxel-based network analyses in resting-state fMRI data," *NeuroImage* **50**(2), 499–508 (2010).

28. R. Milo, O. S. Shen, S. Itzkovitz, N. Kashtan, D. Chklovskii, U. Alon. "Network motifs: Simple building blocks of complex networks," *Science* **298**(5594), 824–827 (2002).

29. M. P. van den Heuvel, C. J. Stam, M. Boersma, H. H. Pol, "Small-world and scale-free organization of voxel-based resting-state functional connectivity in the human brain," *NeuroImage* **43**(3), 528–539 (2008).

30. D. S. Bassett, E. Bullmore, "Small-world brain networks," *Neuroscientist* **12**(6), 512–523 (2006).

31. M. D. Humphries, K. Gurney, T. J. Prescott, "The brainstem reticular formation is a small-world, not scale-free, network," *Proc. R. Soc. Lond. B Biol. Sci.* **273**(1585), 503–511 (2006).

32. J. Zhang, J. Wang, Q. Wu, W. Kuang, X. Huang, Y. He, Q. Gong, "Disrupted brain connectivity networks in drug-naive, first-episode major depressive disorder," *Biol. Psychiatry* **70**(4), 334–342 (2011).

33. B. C. van Wijk, C. J. Stam, A. Daffertshofer, "Comparing brain networks of different size and connectivity density using graph theory," *PLoS One* **5**, e13701 (2010).

34. A. Fornito, A. Zalesky, M. Breakspear, "Graph analysis of the human connectome: Promise, progress, and pitfalls," *NeuroImage* **80**, 426–444 (2013).

35. T. Fekete, F. D. Beacher, J. Cha, D. Rubin, L. R. Mujica-Parodi, "Small-world network properties in prefrontal cortex correlate with predictors of psychopathology risk in young children: A NIRS study," *NeuroImage* **85**, 345–353 (2014).

36. A. M. De Groot, *Bilingual Cognition: An Introduction*, Psychology Press, UK (2011).

37. Y. He, "A fresh cognitive perspective to horizontal translation," *J. Transl. Stud.* **10**(1), 77–90 (2007).